Pergamon

Geochimica et Cosmochimica Acta, Vol. 64, No. 17, pp. 2937–2950, 2000

0016-7037/00 $20.00 + .00

PII S0016-7037(00)00394-X

# An assessment of calcite crystal growth mechanisms based on crystal size distributions

D. E. KILE,* D. D. EBERL, A.R. HOCH,† and M. M. REDDY
U.S. Geological Survey, 3215 Marine St., Ste. E-127, Boulder, CO 80303, USA

(*Received December* 22, 1999; *accepted in revised form February* 28, 2000)

**Abstract**—Calcite crystal growth experiments were undertaken to test a recently proposed model that relates crystal growth mechanisms to the shapes of crystal size distributions (CSDs). According to this approach, CSDs for minerals have three basic shapes: (1) asymptotic, which is related to a crystal growth mechanism having constant-rate nucleation accompanied by surface-controlled growth; (2) lognormal, which results from decaying-rate nucleation accompanied by surface-controlled growth; and (3) a theoretical, universal, steady-state curve attributed to Ostwald ripening. In addition, there is a fourth crystal growth mechanism that does not have a specific CSD shape, but which preserves the relative shapes of previously formed CSDs. This mechanism is attributed to supply-controlled growth.

All three shapes were produced experimentally in the calcite growth experiments by modifying nucleation conditions and solution concentrations. The asymptotic CSD formed when additional reactants were added stepwise to the surface of solutions that were supersaturated with respect to calcite (initial $\Omega = 20$, where $\Omega = 1$ represents saturation), thereby leading to the continuous nucleation and growth of calcite crystals. Lognormal CSDs resulted when reactants were added continuously below the solution surface, via a submerged tube, to similarly supersaturated solutions (initial $\Omega = 22$ to 41), thereby leading to a single nucleation event followed by surface-controlled growth. The Ostwald CSD resulted when concentrated reactants were rapidly mixed, leading initially to high levels of supersaturation ($\Omega > 100$), and to the formation and subsequent dissolution of very small nuclei, thereby yielding CSDs having small crystal size variances.

The three CSD shapes likely were produced early in the crystallization process, in the nanometer crystal size range, and preserved during subsequent growth. Preservation of the relative shapes of the CSDs indicates that a supply-controlled growth mechanism was established and maintained during the constant-composition experiments. CSDs having shapes intermediate between lognormal and Ostwald also were generated by varying the initial levels of supersaturation (initial $\Omega = 28.2$ to 69.2) in rapidly mixed solutions.

Lognormal CSDs were observed for natural calcite crystals that are found in septarian concretions occurring in southeastern Colorado. Based on the model described above, these CSDs indicate initial growth by surface control, followed by supply-controlled growth. Thus, CSDs may be used to deduce crystal growth mechanisms from which geologic conditions early in the growth history of a mineral can be inferred. Conversely, CSD shape can be predicted during industrial crystallization by applying the appropriate conditions for a particular growth mechanism. 

## 1. INTRODUCTION

It is of practical and theoretical importance to understand the factors that influence mechanisms of calcite crystal growth. These growth mechanisms can be interpreted by analyzing crystal size distributions (CSDs; Eberl et al., 1998). Size distributions can influence carbonate reactivity, which plays an important role in the carbon cycle (Berner and Berner, 1996; Milliman et al., 1999; Arvidson and Mackenzie, 1999) and in buffering water chemistry in hydrologic systems (Drever, 1997). For example, carbonate reactivity can control pH in surface waters (Drever, 1997) with resulting impact on mine drainage (Carrucio and Geidel, 1978). In groundwater systems, crystallization of $CaCO_3$ can influence storage, transmissivity, and water quality (Winter et al., 1995) of aquifers. Dissolution and recrystallization of $CaCO_3$ are important to the diagenesis of limestone and other sedimentary rocks (Ridgley, 1986). Chemical engineers are concerned with $CaCO_3$ scaling in industrial processes involving circulating water for cooling (Davis et al., 1995), and the particle size distribution of $CaCO_3$ is an important parameter in the agricultural feed and paper coating industries.

Numerous studies have investigated factors governing the growth of calcite crystals in a variety of synthetic systems. Many of these factors are relevant to industrial crystallization or environmental considerations (Kitano, 1962; Reddy and Nancollas, 1976; House, 1981; Kazmierczak et al., 1982; Busenberg and Plummer, 1986; Reddy, 1986; Kotaki and Tsuge, 1990; Isopescu et al., 1996; Spanos and Koutsoukos, 1998). Whereas such studies have elucidated chemical and thermodynamic aspects governing the crystallization of calcite from aqueous media, none has been able to provide a theoretical basis from which the shapes of calcite CSDs can be predicted accurately. A recent approach presented by Eberl et al. (1998), and a computer program for simulating crystal growth that is based on this approach (Galoper, an acronym for Growth According to the Law of Proportionate Effect and by Ripening), can be used to interpret experimental results for CSDs. This program, written in Microsoft Excel macros, simulates the development of CSD shapes for a variety of crystal growth mechanisms and nucleation conditions.

*Author to whom correspondence should be addressed (dekile@usgs.gov).
†*Present address:* Dept. of Geology, Lawrence University, Appleton, WI, 54912.

The approach followed by Eberl et al. (1998) indicates that CSDs have three basic shapes, as shown in Figure 1: (1) asymptotic, in which the frequencies of the sizes are greatest in the smallest size classes, and exponentially decrease as size increases; (2) lognormal, in which the logarithms of the crystal sizes are normally distributed, but which has a positive skew toward larger sizes if crystal sizes, rather than their logarithms, are plotted; and (3) a universal, steady-state shape[1] which has a skew toward smaller sizes (i.e., negative skew). This approach is in contrast to earlier models that are based on industrial crystallization processes (Randolph and Larson, 1988; Marsh, 1988; Cashman and Marsh, 1988; Cashman and Ferry, 1988; Marsh, 1998) which employ a population balance method that often fails to model the shapes of CSDs (Larson et al., 1985; Kerrick et al., 1991).

According to the approach mentioned above, the three basic CSD shapes can be related to four crystal growth processes: (1) constant-rate nucleation accompanied by surface-controlled growth, thereby generating an asymptotic CSD; (2) decaying nucleation rate accompanied by surface-controlled growth, thereby generating a lognormal CSD; (3) Ostwald ripening, during which larger crystals grow at the expense of smaller, less stable crystals, thereby generating the negatively skewed CSD; and (4) supply- (transport-) controlled growth, during which growth rates are limited by the activity of reactants at the mineral surface. Two other mechanisms described previously (Eberl et al., 1998), random ripening and crystal agglomeration, are not considered here.

In the present study, a series of calcite nucleation and growth experiments were undertaken to test this approach by relating experimental conditions and crystal growth mechanisms to the shapes of CSDs. The goal was to experimentally reproduce the three fundamental CSD shapes that are simulated by the Galoper program, and to elucidate the chemical conditions required for their generation in a mineral system of broad scientific interest.

## 2. CRYSTAL GROWTH MECHANISMS

Asymptotic and lognormal CSDs can be generated mathematically by the Law of Proportionate Effect (LPE; Kapteyn, 1903; Gibrat, 1930). Briefly, this law states that the rate of growth is proportional to linear size times a random number, thereby making growth rate size-dependent. LPE, taken in this study to be a fundamental crystal growth law, leads to size-dependent growth in two regimes.

First, unrestricted size-dependent growth may occur in systems far from equilibrium. This type of growth is termed "surface-controlled" because its rate is limited only by how fast the crystals can grow given an essentially infinite supply of reactants, and not by the rate of reactant supply to the crystal surface. Such growth results in an exponential increase in mean

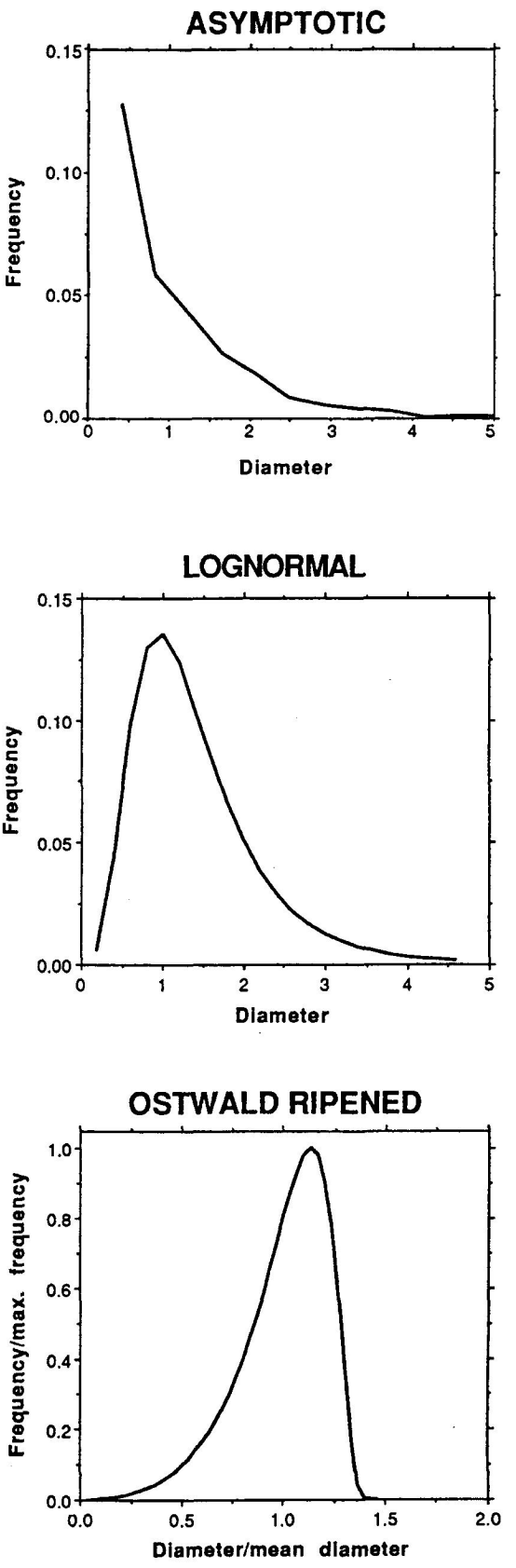


Fig. 1. Three basic shapes of CSDs according to the approach of Eberl et al. (1998).

[1]This shape, attributed to Ostwald ripening (described later), is termed "universal" because it is approached during the ripening process, regardless of the initial shape of the CSD, provided that ripening proceeds far enough. It is called a "steady-state" shape because its shape is constant, regardless of the mean size, when plotted on reduced axes (i.e., size/mean size vs. frequency/maximum frequency). CSDs that have the same steady-state shape have the same logarithmic-based size variance ($\beta^2$).

Table 1. Summary of experimental methods and conditions for calcite crystal growth experiments.

| Sample no. | CSD shapes | Initial vol. (mL) | Initial concentration (M) | | | | | Excess (mL) | Start | Final | | Calculated | |
|---|---|---|---|---|---|---|---|---|---|---|---|---|---|
| | | | $CaCl_2$ | $NaHCO_3$ | $Na_2CO_3$ | $KNO_3$ | NaCl | $CaCl_2$ + KOH | pH[a] | pH | Duration | initial Ω | Final Ω |
| CCNG-2 | asymptotic | 150 | 0.0020 | 0.002 | | 0.093 | | 15 | 8.5 | 8.5 | 100 min | 20 | 22.3 |
| CCNG-30 | asymptotic | 300 | 0.0020 | 0.002 | | 0.093 | | 30 | 8.5 | 8.4 | 195 min | 20 | 17.2 |
| CCNG-35 | lognormal | 300 | 0.0020 | 0.002 | | 0.093 | | 30 | 8.8 | 8.7 | 140 min | 30 | 24 |
| CCNG-40 | lognormal | 300 | 0.0020 | 0.002 | | 0.093 | | 67 | 8.7 | 8.4 | 30 min[a] | 40 | 19 |
| CCNG-42 | lognormal | 300 | 0.0020 | 0.002 | | 0.093 | | 45 | 8.7 | 8.5 | 7 hours[a] | 32 | 21 |
| CCNG-43 | lognormal | 300 | 0.0020 | 0.002 | | 0.093 | | 33 | 8.6 | 8.5 | 230 min[a] | 22 | 18 |
| CCNG-44 | lognormal | 300 | 0.0020 | 0.002 | | 0.093 | | 32 | 8.6 | 8.5 | 5 hours | 22 | 17 |
| CCNG-45 | lognormal | 300 | 0.0020 | 0.002 | | 0.093 | | 64 | 8.8 | 8.5 | 225 min[a] | 41 | 26 |
| CCNG-9 | Ostwald | 100 | 0.0265 | 0.002 | 0.0244 | 0.046 | | | 10.7 | 10.0 | ~1 min | 3090[c] | [b] |
| CCNG-13 | Ostwald | 100 | 0.0265 | 0.002 | 0.0244 | 0.046 | | | 10.7 | 8.4 | 14 hours | 3090[c] | 42 |
| CCNG-19 | Ostwald | 400 | 0.0050 | | 0.0050 | | 0.50 | | 10.5 | 10.0 | 40 min | 106 | 67 |
| CCNG-20 | Ostwald | 200 | 0.0265 | 0.002 | 0.0244 | 0.046 | | | 10.5 | 8.1 | 90.5 hours | 3090[c] | 2 |
| CCP-4[d] | Ostwald | 400 | 0.0020 | 0.002 | | 0.093 | | | 8.5 | 8.5 | 45 hours | 5 | 5 |
| 7-26 | transitional | 400 | 0.0025 | | 0.0025 | 0.025 | 0.25 | | 10.3 | 10.3 | 53 min | 28.2 | [b] |
| 7-12 | transitional | 400 | 0.0038 | | 0.0050 | 0.05 | 0.50 | | 10.5 | 10.5 | 50 min | 53.7 | [b] |
| 7-20 | transitional | 400 | 0.0050 | | 0.0050 | 0.05 | 0.50 | | 10.3 | 10.3 | 49 min | 69.2 | [b] |
| CCNG-25 | bimodal | | 0.0050 | 0.005 | | | 0.50 | | 9.9 | 9.7 | 105 min | 51.4 | 10.5 |

[a] In lognormal experiments, the time listed is the time from highest pH to final sampling.
[b] $Ca^{2+}$ concentration data not available for calculation.
[c] Actual value of omega does not exceed ~100 due to short induction time.
[d] Constant composition experiment using CCNG-19 crystals as seed.

crystal size and a linear increase in crystal size variance ($\beta^2$, defined in "Experimental Methods") with time. Each individual crystal's growth rate is governed by its size ($X_j$) and a random variable ($\epsilon_j$) that generally varies between zero and one. The range of $\epsilon_j$ is an indication of system variability, and, in the Galoper program, its values are evenly distributed:

$$X_{j+1} = X_j + \epsilon_j X_j. \quad (1)$$

Equation 1 is iterated many times for each crystal, with each iteration termed a growth cycle. After several growth cycles involving many crystals, a lognormal CSD results. LPE growth requires an exponentially increasing amount of nutrients as the number of growth cycles (or time) increases, a demand that quickly exceeds a system's capacity to supply reactants. Then supply-controlled growth (described below) commences, presumably while the crystals are in the nm size range.

During surface-controlled LPE growth, crystals are subjected both to size-dependent growth (during which larger crystals tend to grow faster), and to crystal size dispersion (during which crystals having the same initial size may grow at different rates). Both processes are represented in the $\epsilon_j X_j$ term in Eqn. 1, where $X_j$ manifests size dependence, and the range in $\epsilon_j$ influences dispersion.

Whereas surface-controlled LPE growth produces a lognormally shaped CSD, an asymptotic CSD develops if new nuclei are added to a system at a constant rate as LPE growth proceeds. When nucleation ceases, the asymptotic CSD may evolve toward a lognormal shape by continued LPE growth. Lognormal-shaped CSDs also can be produced by surface-controlled (LPE) growth in systems having a decaying nucleation rate. During this mechanism, nucleation gradually subsides while previously nucleated crystals continue LPE growth, leading to a pseudo-lognormal or to a lognormal-shaped CSD. How closely the CSD approaches a true lognormal distribution depends on the duration of LPE growth following nucleation.

The second regime for size-dependent growth is governed by a supply-controlled mechanism. Crystals grow according to a modified version of the LPE, during which there is a smaller tendency for growth dispersion (i.e., a smaller range for $\epsilon_j$). This type of growth leads to a decreasing rate of growth with increasing mean size, and to a constant size variance (i.e., $\beta^2$ = constant). The volume increase of each crystal ($\Delta V_j$) is limited by the availability of reactants, whereby the unconstrained growth volume demanded by Eqn. (1) for each crystal ($\Delta V_{j,LPE}$) is reduced proportionately by the ratio of total volume allowed for each growth cycle for all crystals in the system ($\Sigma\Delta V_a$) to the total volume required for all crystals by unconstrained LPE growth ($\Sigma\Delta V_{j,LPE}$):

$$\Delta V_j = (\Delta V_{j,\mathrm{LPE}}) \frac{\sum \Delta V_a}{\sum \Delta V_{j,\mathrm{LPE}}}. \quad (2)$$

$\Delta V_j$ is added to the volume of the previous crystal, and the new crystal dimension is calculated for use in Eqn. 1. This growth mechanism does not in itself generate a distinctive CSD shape, but rather, preserves the size variance and relative shape of a previously established CSD (e.g., asymptotic, lognormal, etc.) as crystal growth continues. This shape is preserved because the $\Delta V_j$ term in Eqn. 2 generally is very small, leading to a small growth term ($\epsilon_j X_j$) in Eqn. 1. Therefore, although size-dependent growth continues during supply-controlled growth, there is little tendency for growth dispersion, and the growth rate can be approximated as $dX/dt = kX$ (see also Nordeng and Sibley, 1996).

Growth by LPE (both by surface-control and by supply-control mechanisms) is in distinct contrast to traditional crystal growth theory which expresses crystal growth rates as mass per unit surface area per unit time, and therefore, assumes that linear growth rate is independent of crystal size (e.g., $dX/dt$ =

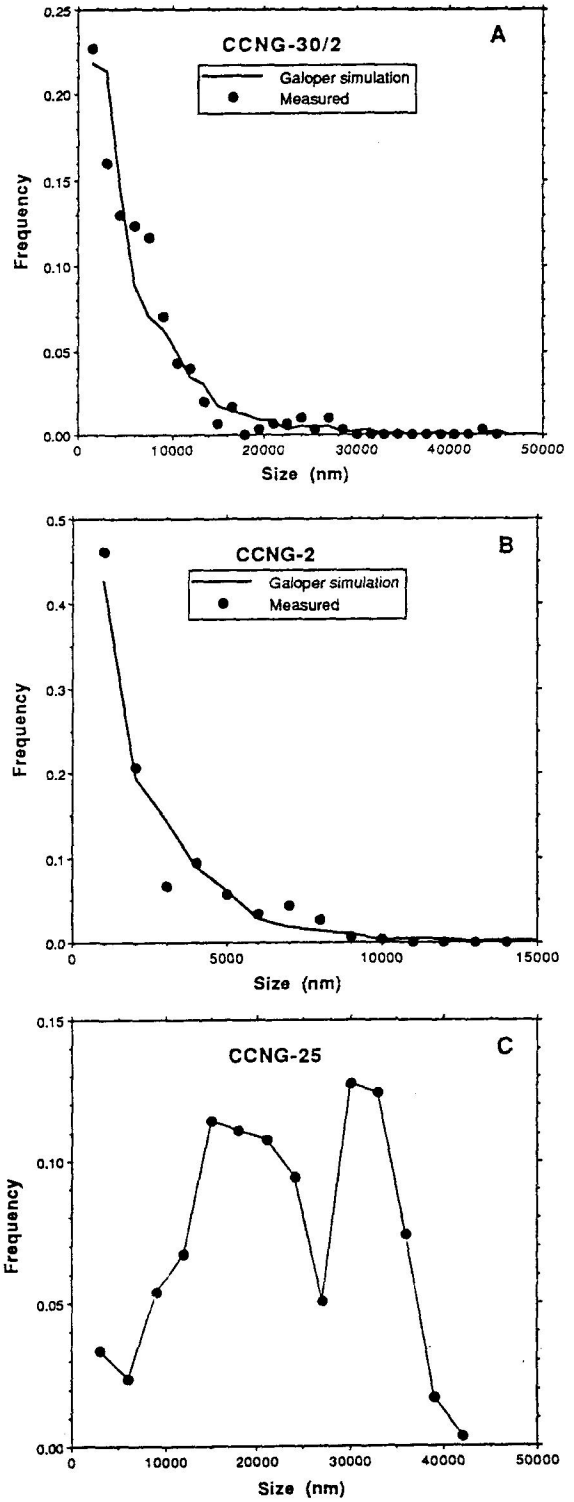


Fig. 2. (A) Characteristic asymptotic CSD for sample CCNG-30/2. The Galoper simulation used a critical nucleus size of 3 nm (read from Fig. 10, using $\Omega = 20$ from Table 1) with 143 crystals nucleating per calculation cycle, followed by supply-controlled growth to the correct mean size; level of significance for $\chi^2$ comparison between simulated and measured CSDs = 2.5 to 5%. (B) Characteristic asymptotic CSD for sample CCNG-2. CSD simulated as in A, with significance level = 1 to 5%. (C) Bimodal CSD resulting from sequential addition of $CaCl_2$ and KOH for sample CCNG-25.

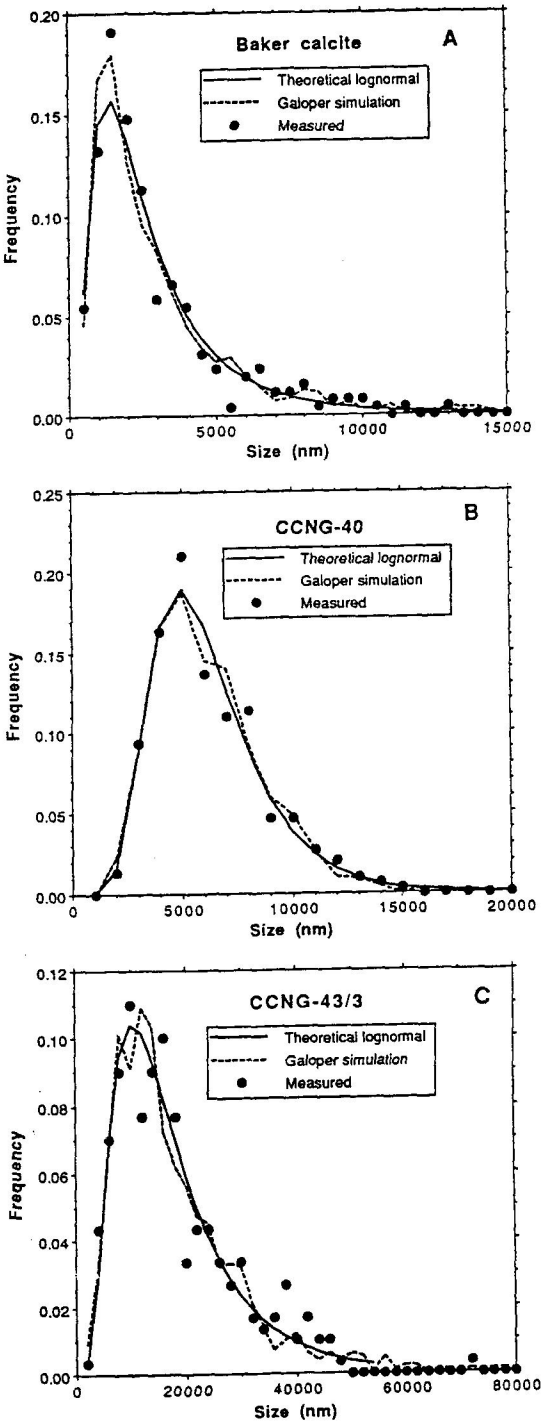


Fig. 3. (A) Plot of size vs. frequency showing lognormal CSD for Baker calcite. Galoper simulation used a critical nucleus size of 3 nm and a probability for nucleation of 0.6, followed by supply-controlled growth; significance level for $\chi^2$ comparison between simulation and measurements = 10 to 20%. (B) Plot of size vs. frequency for a typical lognormal profile of synthetically grown calcite (CCNG-40). Galoper simulation used a critical nucleus size of 2.5 nm (Table 1 and Fig. 10) and a probability for nucleation of 0.85, followed by supply-controlled growth; significance level > 20%. (C) Plot of size vs. frequency for a typical lognormal profile of synthetically grown calcite (CCNG-43/3). Galoper simulation used a critical nucleus size of 3 nm (Table 1 and Fig. 10), and a probability for nucleation of 0.60; significance level > 20%.

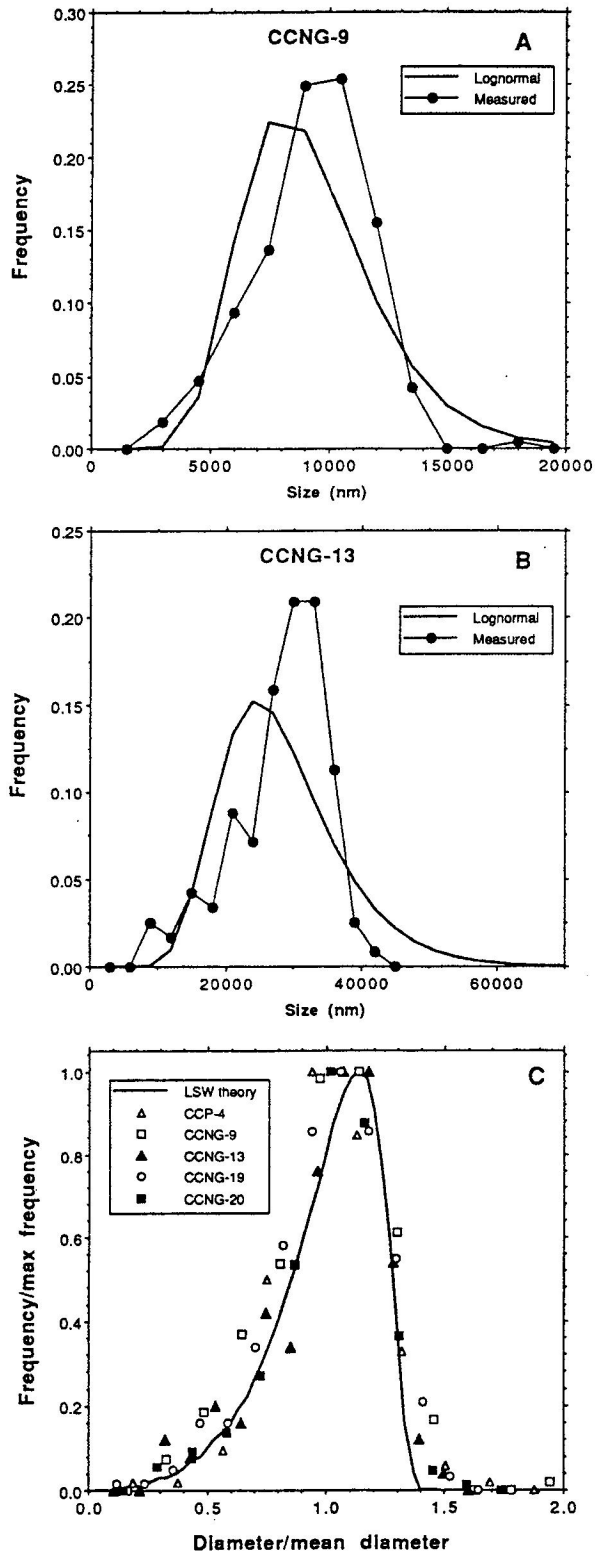


Fig. 4. (A) Negatively skewed CSD characteristic of Ostwald ripening (CCNG-9). (B) Negatively skewed CSD characteristic of Ostwald ripening (CCNG-13). (C) Reduced plot showing ripened samples with the theoretical, universal, steady-state curve expected for diffusion-controlled Ostwald ripening according to the LSW theory, with ripened samples.

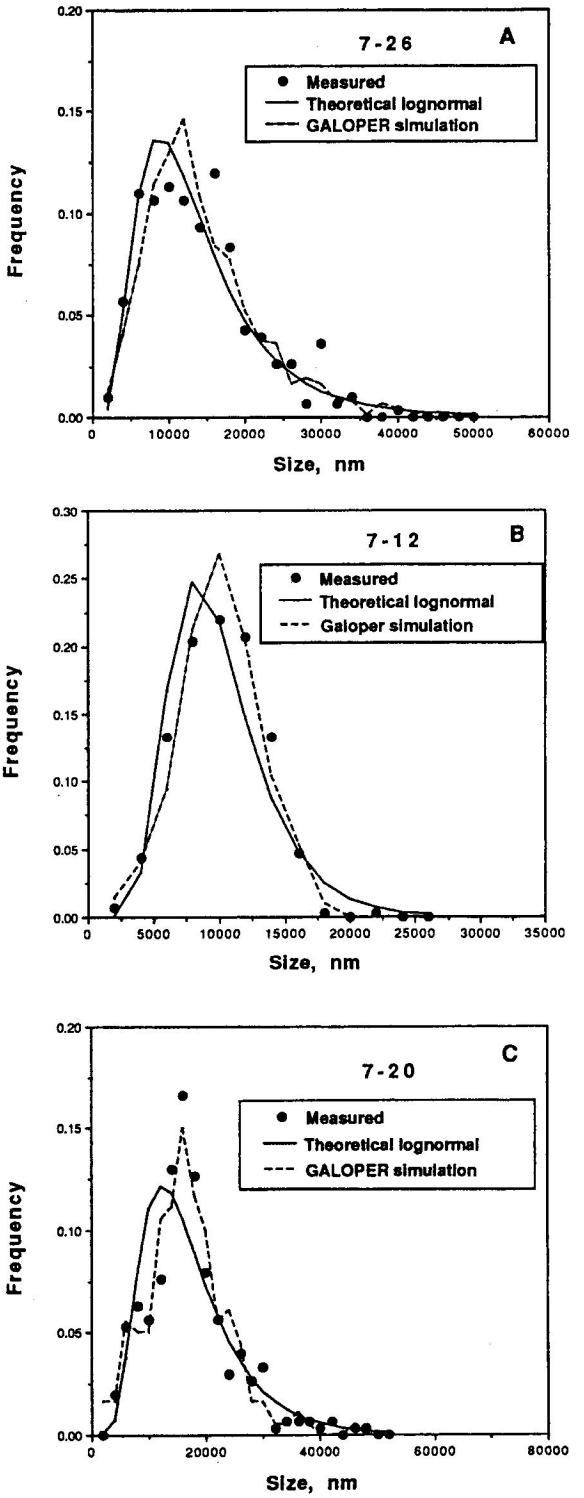


Fig. 5. (A) Transitional CSD (sample 7-26) with a shape that is intermediate between lognormal and Ostwald curves. Starting $\Omega$ = 28.2. $\chi^2$ significance between experimental data and Galoper simulation = 5 to 10%. (B) Transitional CSD (sample 7-12) with a shape that is intermediate between lognormal and Ostwald curves. Starting $\Omega$ = 53.7. $\chi^2$ significance between experimental data and Galoper simulation = 10 to 20%. (C). Transitional CSD (sample 7-20) with a shape that is intermediate between lognormal and Ostwald curves. Starting $\Omega$ = 69.2. $\chi^2$ significance between experimental data and Galoper simulation = > 20%.

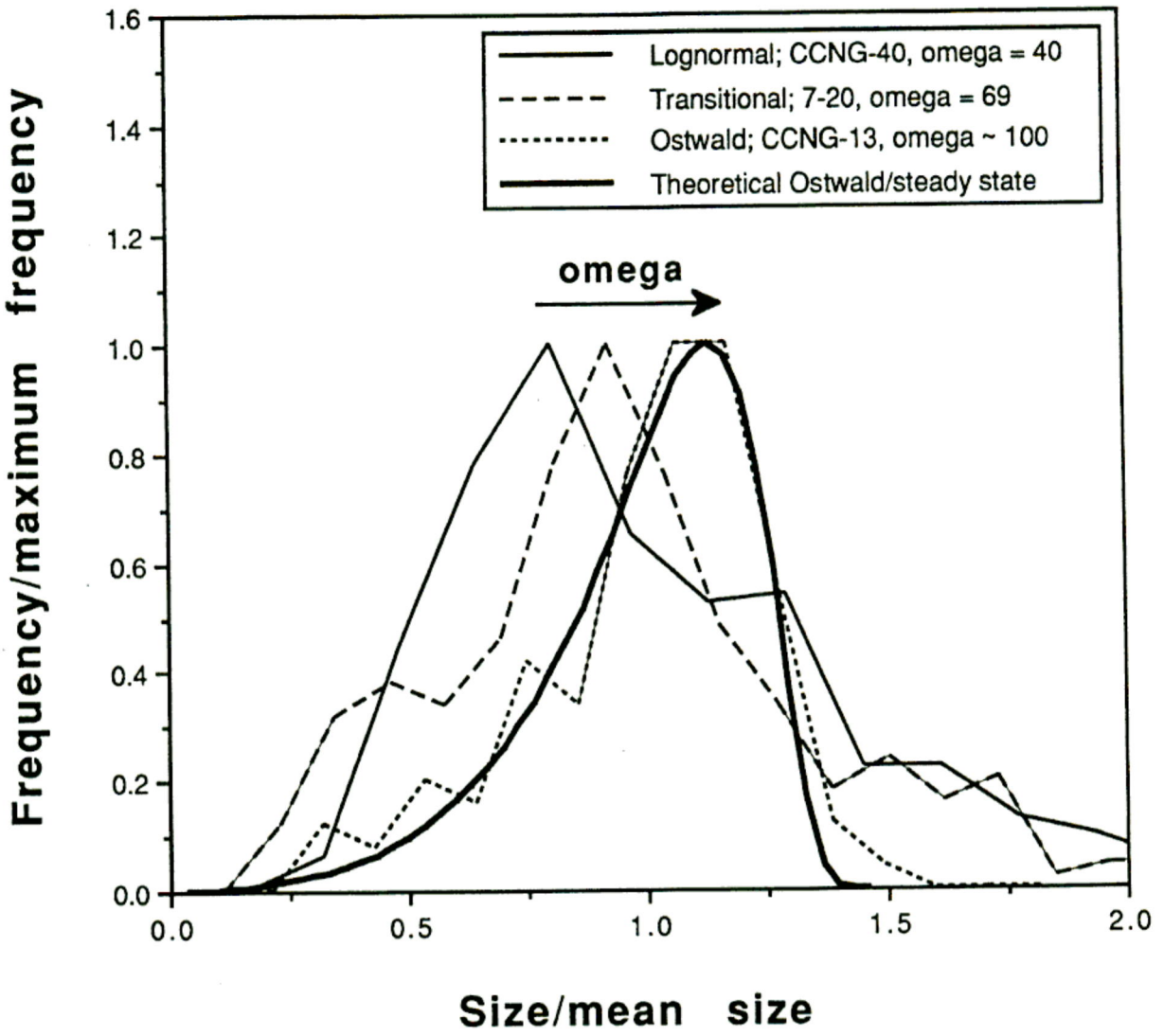


Fig. 6. Reduced plot of lognormal, transitional, and Ostwald CSDs showing a progressive shift with increasing $\Omega$ toward the theoretical Ostwald steady-state curve.

$k$; see Nielsen, 1964). This approach is exemplified by McCabe's law (McCabe, 1929), which states that geometrically similar crystals in the same solution will grow at the same linear rate. Therefore, this kinetic theory infers that the absolute size differences between crystals are maintained as growth proceeds, an important consequence of which is a diminishing crystal size variance ($\beta^2$) with time. Surface-controlled LPE growth, however, mandates that crystal size variance increases with mean diameter, because the range of values possible for $\epsilon_j$ in Eqn. 1 leads to crystal size dispersion. Conversely, supply-(transport-) controlled LPE growth mandates that variance remains constant during growth. There is a growing body of experimental evidence that supports crystal size dispersion (for sucrose, White and Wright, 1971), and size-dependent growth for a variety of synthetic crystal systems, e.g., Canning and Randolph, 1967 ($Na_2SO_4 \cdot 10H_2O$); Garside and Jančić, 1976 [$KAl(SO_4)_2 \cdot 12H_2O$]; Berglund et al., 1983 ($KNO_3$); Tai and Yu, 1989 [$KAl(SO_4)_2 \cdot 12H_2O$]; and Tai et al., 1993 ($CaCO_3$), as well as in geologic systems, e.g., Nordeng and Sibley, 1996, and Makowitz and Sibley, 1999.

According to LSW theory [Lifshitz and Slyozov (1961), and Wagner (1961)], a specific, negatively skewed shape is produced by diffusion-controlled Ostwald ripening. During this process, the smallest crystals, rendered unstable by their large specific surface free energy and by a falling level of supersaturation in solution, dissolve to yield material for growth of larger crystals. The overall growth rate is determined by the rate of reactant supply to the larger crystals (e.g., by the rate of dissolution of smaller crystals).

## 3. EXPERIMENTAL METHODS

Experiments were performed in a 400 mL double-walled glass reactor vessel connected to a circulating water bath which maintained a constant temperature of 25.0 ± 0.2°C. The reactor was covered but not sealed. A propeller rotating at 250 to 300

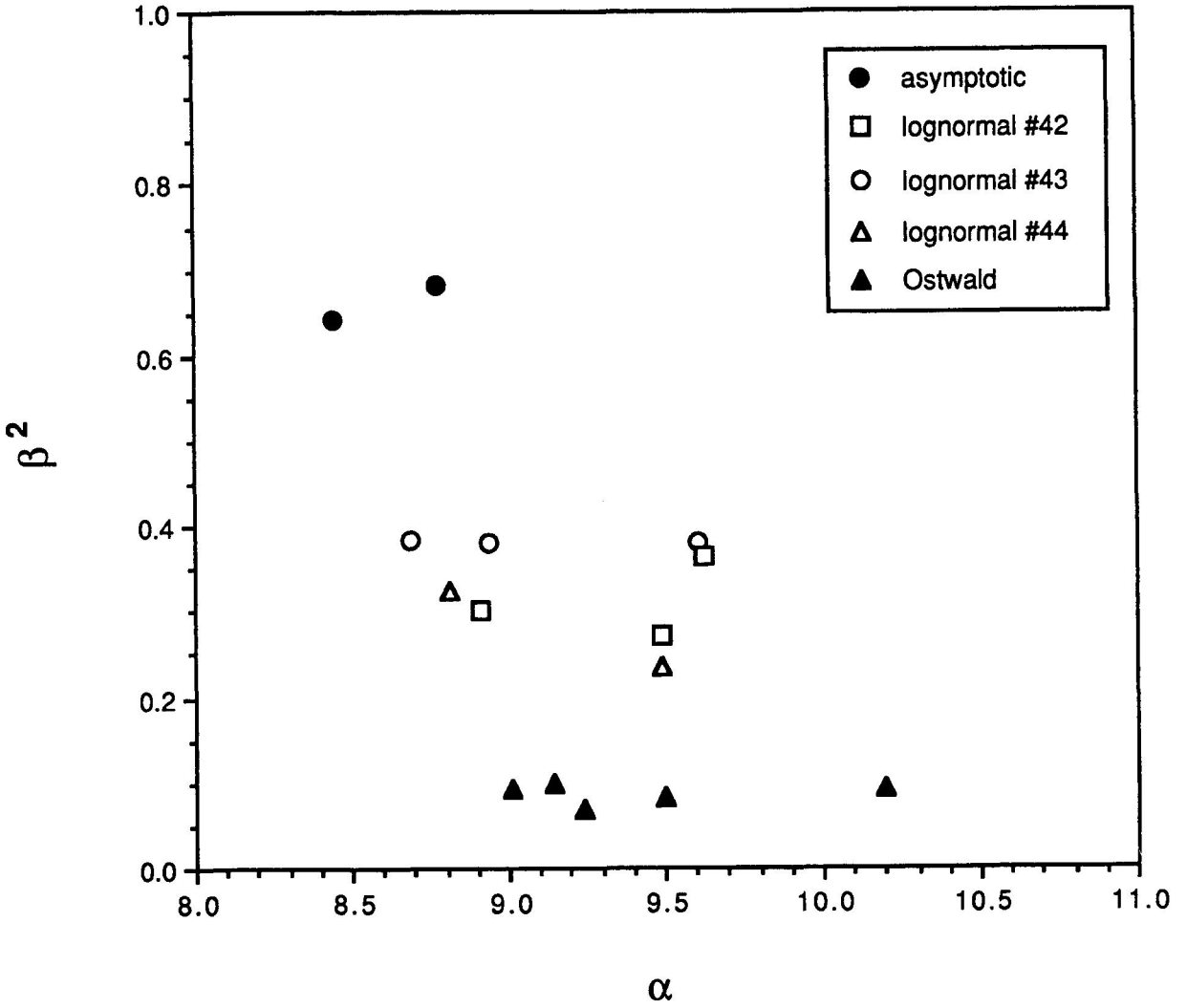


Fig. 7. Plot of size variance ($\beta^2$) vs. natural log mean size ($\alpha$) for synthetic calcite.

rpm was used for mixing in the reactor vessel to avoid grinding crystals (which may occur with a magnetic stir bar) during all experiments except CCNG-9. All solutions were filtered through 0.1 $\mu$m cellulose nitrate (CN) filters prior to the experiment and were used within 36 h. Initial $Ca^{2+}$ concentration in the $CaCl_2$ solutions was measured by ethylenediaminetetraacetic acid (EDTA)/calcein titration (Diehl, 1964) to adjust for variable hydration effects of the stock $CaCl_2 \cdot 2H_2O$. Table 1 shows the starting concentrations of $CaCl_2$ and $NaHCO_3$, and includes $KNO_3$ that was added to regulate ionic strength.

Constant composition experiments were performed to simulate supply-controlled growth, and were based on the method of Tomson and Nancollas (1978), where pH, $[Ca^{2+}]$, and $[CO_3^{2-}]$ were kept at a constant level throughout the experiment to maintain an invariant level of supersaturation ($\Omega$), defined as:

$$\Omega = Q/K_{sp}, \tag{3}$$

where

$$Q = [H^+]/[Ca^{2+}][HCO_3^-], \tag{4}$$

in which the brackets refer to activities in solution, and $K_{sp}$ is the solubility product of calcite crystals in the standard state (i.e., crystals having an essentially infinite particle size). Solution speciation and $\Omega$ were calculated using either the WATEQ4F program of Ball and Nordstrom (1991) or the PHREEQC program of Parkhurst (1995).

Constant composition conditions were achieved using a Brinkmann pH-stat titration system, where equal volumes of equimolar $CaCl_2$ and $Na_2CO_3$ solutions containing $KNO_3$ (Table 1) were added to the reactor vessel at a rate equal to the growth rate of the crystals. Thus, as reactants were depleted during crystal growth (accompanied by a drop in pH), titrant solutions were automatically added to maintain a constant pH of 8.5. The volumes of titrants added and pH were monitored continuously throughout the experiment to provide growth rate data.

Both vaterite (the hexagonal polymorph of $CaCO_3$) and

calcite (trigonal $CaCO_3$) crystallized during the experiments, but in all but three experiments the amount of vaterite was considerably subordinate to that of calcite. The presence of vaterite did not appear to influence the shape of calcite CSDs because the CSD shape was independent of the presence of vaterite and consistent with that expected for the experimental conditions. Attempts were made to suppress noncalcite phases in the higher $\Omega$ experiments (Table 1) by adding high (0.5 M) concentrations of NaCl (Kitano, 1962), with varied success. Crystallization of aragonite (the orthorhombic $CaCO_3$ polymorph) is not favored under ambient temperature conditions in the absence of $Mg^{2+}$, and was not found optically or by X-ray diffraction.

After completion of an experiment, solutions and crystals were filtered immediately through a 0.45 $\mu$m CN filter, and the reaction-product crystals dried in air at 40°C for approximately 30 min. Samples were removed mechanically from the CN filter and placed on a 27 × 46 mm glass slide; a coverslip was then added using Canada balsam. Crystal size was measured with a conventional petrographic microscope using a filar micrometer ocular (total magnification ~500×) and partly crossed polars to utilize properties of birefringence and variable relief to improve definition of crystal edges. Measurement using optical light-scattering devices (e.g., Coulter counter, Malvern Zetasizer) overestimated crystal size by factors varying from 2 to 6, a likely result of measurement of crystal aggregates as coherent units.

Synthetic crystals were measured on their long diagonal; measurements were averaged for very asymmetric rhombohedra, although most crystals were equant in habit. Approximately 300 crystals were measured per sample. This method of measurement was validated for a calcite sample from the Baker Chemical Co. (catalog no. 1288) by comparing the surface area calculated from the shape of the CSD (0.31 $m^2/g$) with that measured by the nitrogen Brunauer-Emmett-Teller (BET) method (0.256 ± 0.008 $m^2/g$).

CSDs also were determined for calcite crystals found within septarian concretions in an Upper Cretaceous shale in southeastern Colorado. These crystals were measured on a diagonal using either a millimeter scale or a stereomicroscope with a calibrated ocular micrometer.

CSDs were calculated from crystal size data using the program CrystalCounter, written in Microsoft Excel macro language. Because group size can influence the chi-square ($\chi^2$) fit of the lognormal distribution (see below), it is important to have a consistent rationale in selecting this parameter. In general, group size was set to a minimum that barely mitigated the "noise" level in the plot, resulting in most experiments having a group size that was about one-fifth of the mean crystal size. The program then calculates the CSD shape, the mean crystal size, the mean of the natural logarithms of the sizes [$\alpha = \Sigma \ln(X) f(X)$, where $\ln(X)$ is the natural logarithm of the crystal group size, and $f(X)$ is the frequency of crystals for that size], and the variance of the natural logarithms of the sizes [$\beta^2 = \Sigma(\ln X - \alpha)^2 f(X)$]. The sensitivity of $\beta^2$ to the presence of very small crystals at the limit of optical resolution (less than ~ 1 $\mu$m) limits the precision of the size variance calculation.

The $\chi^2$ test (Krumbein and Graybill, 1965) was used to assess the lognormal fit of the data. This test compares differential curves of theoretical lognormal vs. measured size distributions, and gives a level of significance ranging from <1% (lognormal fit is not significant) to >20% (high level of significance). CSDs are considered to be lognormal if the significance level for comparison between the measured and theoretical curves is equal to or greater than the 1 to 5% range (Exner and Lukas, 1971).

## 4. EFFECTS OF CRYSTAL GROWTH METHODS ON CSD SHAPES

Asymptotic CSDs (Figs. 2A,B) were produced by stepwise addition (by pipette) of concentrated (excess) $CaCl_2$ solution to the surface of moderately supersaturated solutions ($\Omega$ = 20; see Table 1). The excess calcium solution was added 5 to 10 times over the course of 20 to 60 min, followed by pH adjustments with KOH after each addition. The pH was allowed to stabilize for several minutes after each addition, and then was adjusted to 8.5 using 0.05 M KOH. Presumably multiple nucleation events were triggered by the stepwise additions of highly concentrated $CaCl_2$ solution and/or KOH to the surface of the solution, both of which would increase the local level of supersaturation. The addition of excess $CaCl_2$ was discontinued when pH no longer would stabilize, but continued to decrease. This spontaneous decrease in pH likely was related to calcite growth, and at this point calcite crystals could be observed microscopically.

A bimodal CSD developed from a similar experiment (Fig. 2C), but which had only two KOH additions, separated in time by 30 min (Table 1). This experiment verified the premise that distinct nucleation events would be expressed in the resultant CSD.

Crystals having lognormal CSDs were grown by a method similar to that used for the asymptotic experiments, but in contrast to the stepwise addition of reactants to the solution surface, excess $CaCl_2$ and KOH were added through a submerged tube with a peristaltic pump at a flow rate of approximately 0.3 mL/min (except for the CCNG-35 experiment, during which excess $CaCl_2$ and KOH were added rapidly by volumetric pipette); initial solution $\Omega$ values ranged between 22 and 41 (Table 1). In these experiments, the continuous (rather than incremental) addition of reactants over the course of 0 to 170 min presumably resulted in a single nucleation event that was followed by LPE growth. Crystals then were allowed to grow with no further solution additions until the pH dropped to 8.5, after which constant composition/supply-controlled growth was initiated and maintained by the constant composition method of Tomson and Nancollas (1978). A lognormal CSD for a commercially prepared calcite (Baker Chemical Co.) is presented in Figure 3A for comparison with our experiments (Figs. 3B and 3C).

In several experiments (CCNG 42, 43, and 44), sequential samples were taken at timed intervals to assess the effect of continued growth (i.e., larger mean diameter) on the CSD shape and size variance. Generally, the relative lognormal shape and $\beta^2$ remained approximately constant, as would be expected for supply-controlled growth.

CSDs having the shape typical for Ostwald ripening (i.e., a curve that is overall shifted right from the theoretical lognormal curve and that has a left-skewed tail; see Fig. 4) were obtained by rapid mixing of equimolar solutions of $Ca^{2+}$ and $CO_3^{2-}$

Table 2. Crystal size distribution data and statistical evaluation for calcite crystal growth experiments; horizontal lines indicate continuous growth experiments.

| CSD shape | Sample no. | $\alpha$ | $\beta^2$ | Group size | Average size (nm) | Lognormal significance, $\chi^2$ test |
|---|---|---|---|---|---|---|
| asymptotic | CCNG-30/2 | 8.45 | 0.64 | 1,500 | 6,420 | NA |
| asymptotic | CCNG-30/3 | 8.78 | 0.68 | 1,700 | 8,864 | NA |
| asymptotic | CCNG-2 | 7.60 | 0.52 | 1,000 | 2,585 | NA |
| lognormal | CCNG-42/1 | 8.91 | 0.30 | 1,000 | 8,500 | 2.5–5 |
| ~lognormal | CCNG-42/2 | 9.49 | 0.27 | 2,000 | 14,870 | <1 |
| lognormal | CCNG-42/3 | 9.62 | 0.36 | 1,500 | 17,810 | 10–20 |
| lognormal | CCNG-43/1 | 8.69 | 0.38 | 2,000 | 7,140 | >20 |
| lognormal | CCNG-43/2 | 9.00 | 0.49 | 2,000 | 10,320 | 1–5 |
| lognormal | CCNG-43/3 | 9.61 | 0.38 | 2,000 | 17,853 | >20 |
| lognormal | CCNG-44/1 | 8.81 | 0.32 | 2,000 | 7,950 | >20 |
| lognormal | CCNG-44/2 | 9.49 | 0.23 | 2,000 | 14,800 | >20 |
| lognormal | CCNG-40 | 8.65 | 0.16 | 1,000 | 6,200 | >20 |
| lognormal | CCNG-45/3 | 9.33 | 0.25 | 2,700 | 12,690 | 10–20 |
| lognormal | CCNG-35 | 9.03 | 0.32 | 2,000 | 9,770 | >20 |
| lognormal | Baker calcite | 7.72 | 0.59 | 500 | 2,944 | 10–20 |
| Ostwald | CCNG-9 | 9.14 | 0.10 | 1,500 | 9,359 | NA |
| Ostwald | CCNG-13 | 10.20 | 0.09 | 3,000 | 28,080 | NA |
| Ostwald | CCNG-19 | 9.01 | 0.09 | 1,000 | 8,522 | NA |
| Ostwald | CCNG-20 | 9.50 | 0.08 | 2,000 | 13,792 | NA |
| Ostwald | CCP-4 | 9.24 | 0.07 | 2,000 | 10,640 | NA |
| transitional | 7-26 | 9.40 | 0.31 | 2,000 | 13,953 | NA |
| transitional | 7-12 | 9.15 | 0.13 | 2,000 | 10,040 | NA |
| transitional | 7-20 | 9.65 | 0.24 | 2,000 | 17,294 | NA |
| bimodal | CCNG-25 | 9.93 | 0.25 | 3,000 | 22,812 | NA |

NA = not applicable.

(Table 1), resulting in working solutions with relatively high supersaturation levels ($\Omega > 100$), in contrast to the lower initial $\Omega$ values (20 to 41) for the asymptotic and lognormal experiments. The "nominal" initial supersaturation levels were calculated to have $\Omega$ = 106 to 3090. There is experimental evidence, however, that the actual $\Omega$ cannot exceed a level of 80 to 100 because of a very short induction time (Söhnel and Mullin, 1987). In other words, the rate of crystallization exceeds the mixing velocity so that crystal precipitation limits the actual $\Omega$ values to about 100. The data shown in Figs. 4A,B do not fit either the asymptotic or theoretical lognormal curves. However, data for all five Ostwald experiments closely approach the shape of the universal steady-state curve expected for diffusion-controlled Ostwald ripening, according to the LSW theory (Lifshitz and Slyozov, 1961; Wagner, 1961), when plotted on reduced axes (i.e., normalized to mean crystal size and maximum frequency; see Fig. 4C).

Continued growth of previously Ostwald ripened crystals was achieved in a subsequent experiment by adding seed crystals of a previously ripened sample (CCNG-19) to a supersaturated solution and then by allowing the crystals to grow at constant pH and solution composition. The reduced shape of the CSD for these crystals (CCP-4) remained constant (i.e., $\beta^2$ did not change appreciably) while the mean size increased from 8.5 to 10.6 $\mu$m, thereby indicating that supply-controlled growth followed Ostwald ripening.

Size distributions having shapes intermediate to lognormal and Ostwald CSDs (Fig. 5) were generated in a similar manner, but initial $\Omega$ values were adjusted to values between 28.2 and 69.2. This transition is demonstrated clearly in Figure 6, where the CSDs progressively approach the theoretical Ostwald curve with increasing $\Omega$.

A plot of $\alpha$ vs. $\beta^2$ for the experimental data (Fig. 7 and Table 2) reveals that the three types of CSD shapes (asymptotic, lognormal, and Ostwald) differ in their overall size variance, with their mean $\beta^2$ values equal to 0.61, 0.32, and 0.086, respectively. This difference in variance is readily discernible under the optical microscope and by scanning electron microscope (SEM). For example, an SEM photograph of a sample (Baker calcite, Fig. 8A) having a lognormally shaped CSD with a variance of 0.52 has a distinctly variable crystal size compared to the relatively uniform crystal size of an Ostwald ripened sample having a variance of 0.09 (Fig. 8B).

CSDs from naturally occurring calcite crystals (Fig. 9) have a lognormal distribution (with levels of significance in the $\chi^2$ test > 10%) for two crystal populations having very different mean sizes, i.e., 2.6 mm and 6.4 mm.

## 5. DISCUSSION

The results shown in Table 2 indicate that all three theoretical shapes (asymptotic, lognormal, and Ostwald) were generated in these experiments. The asymptotically shaped distributions (Fig. 2), formed when reactant solution was added to the

A.

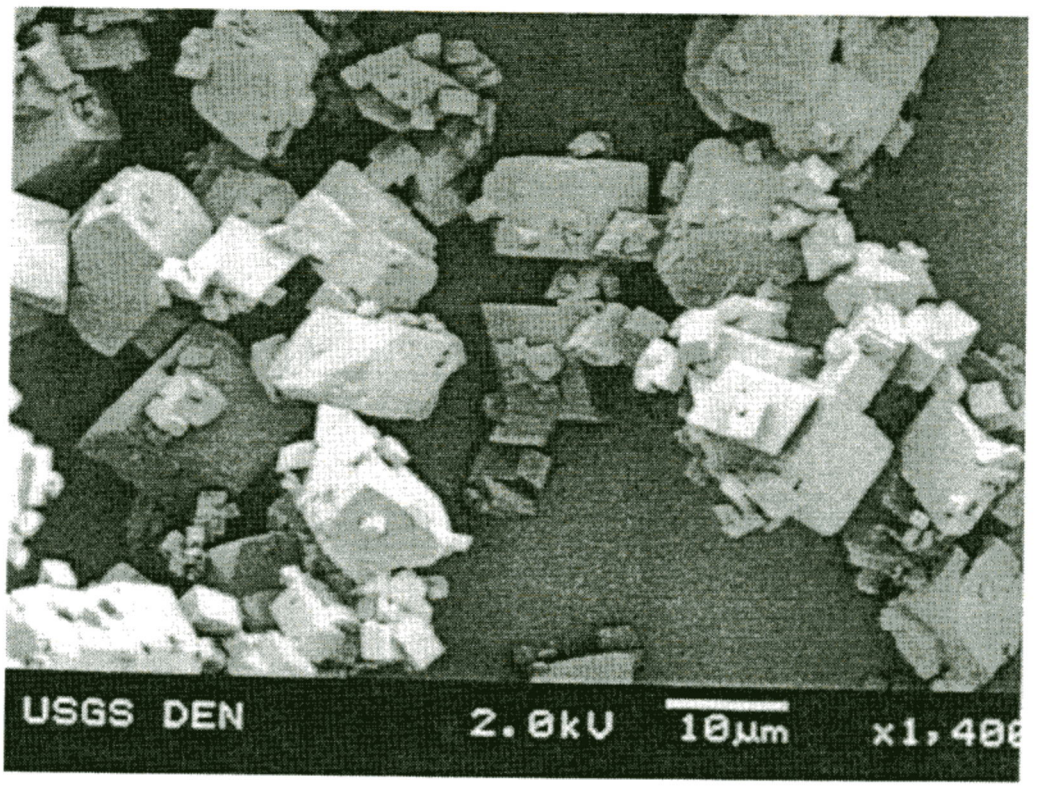


B.

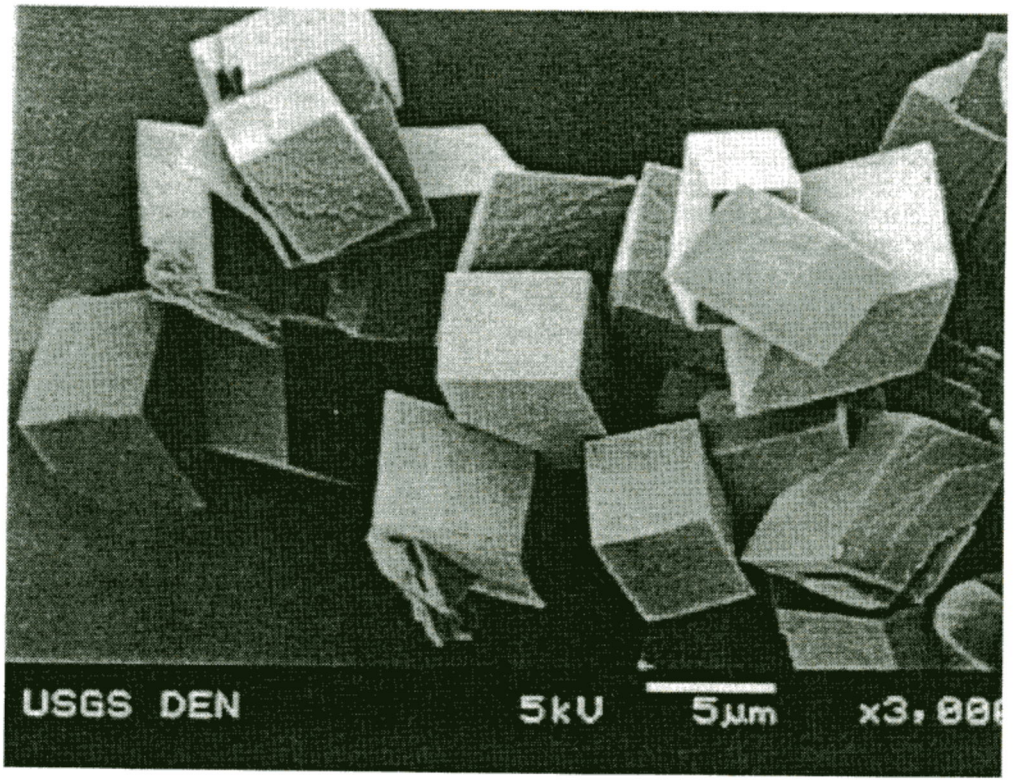


Fig. 8. (A) SEM photo of synthetic calcite (Baker) illustrating a lognormal CSD with large size variance ($\beta^2 = 0.52$). (B) SEM photo of synthetic calcite (CCNG-19) illustrating an Ostwald CSD with a small size variance ($\beta^2 = 0.09$).

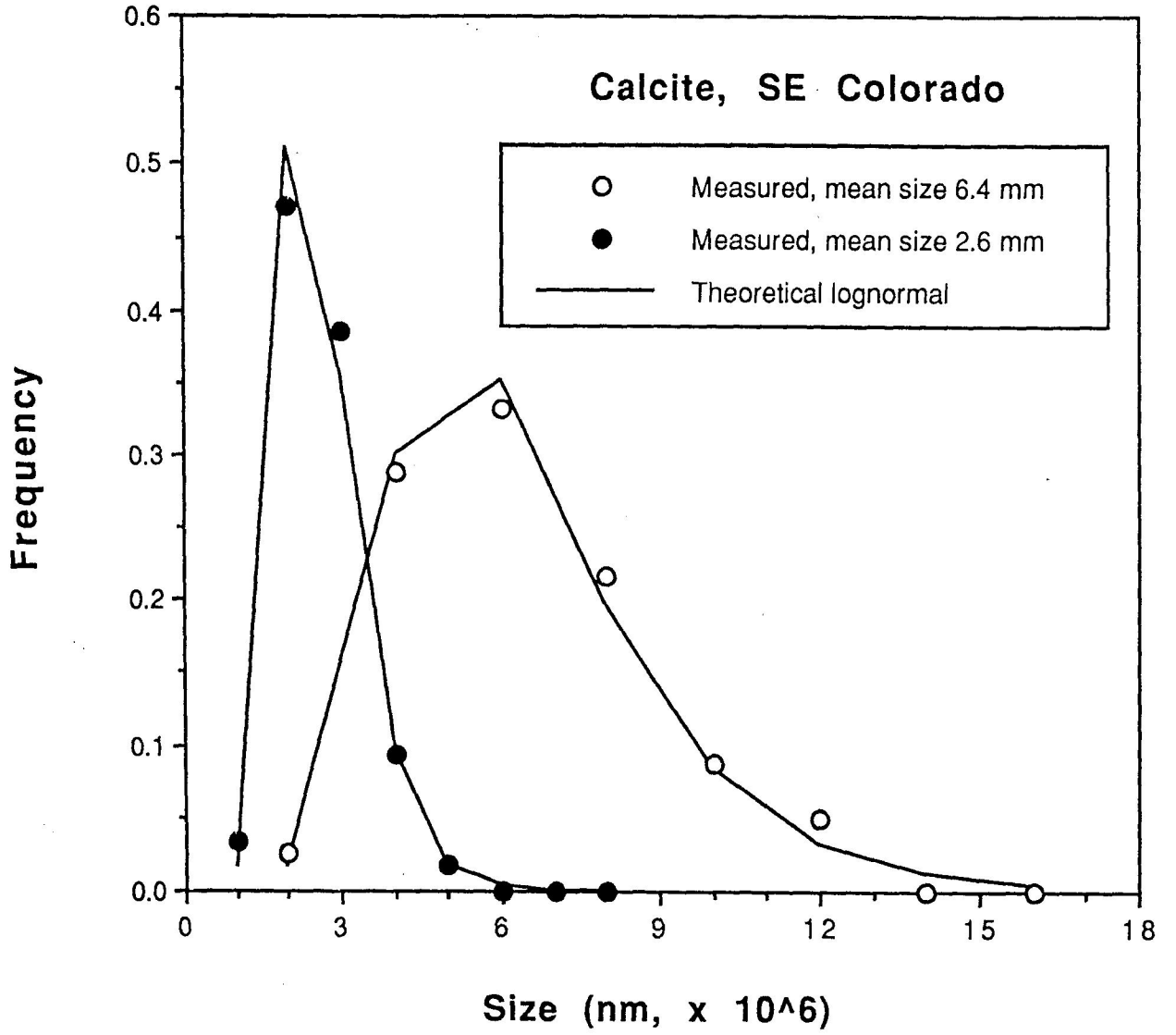


Fig. 9. Lognormal size distributions for two naturally occurring calcite samples from southeastern Colorado.

experiments in a series of increments, are readily explained if new calcite nuclei were formed during each addition. The incremental formation of new crystals, accompanied by the simultaneous growth of larger crystals by size-dependent, LPE growth, leads to a predominance of small crystal sizes, and to an exponential increase in $\beta^2$ as $\alpha$ increases (Eberl et al., 1998). Such a mechanism accounts for the large size variance for this type of CSD (Fig. 7). Galoper simulated CSDs, calculated according to the mechanism of constant-rate nucleation and LPE growth (followed by supply-controlled growth as will be discussed below) are presented for comparison with the experimental data (Figs. 2A,B).

The lognormally shaped CSDs, formed by the gradual addition of reactant solutions, are generated experimentally as the nucleation rate decays and surface-controlled LPE growth continues. LPE growth with a decaying nucleation rate leads to a linear increase in $\beta^2$ as $\alpha$ increases, thereby accounting for the intermediate size variance for this type of CSD (Fig. 7). The Galoper simulated curves for this mechanism are presented in Figures 3B,C.

The CSD shapes attributed to Ostwald ripening closely fit the theoretical universal steady-state curve predicted by the LSW theory (Fig. 4C). The small crystal size variances (Fig. 7) are attributed to this process, during which $\beta^2$ decreases toward a constant, theoretical minimum value (based on Galoper calculations) of about 0.06.

The presence of Ostwald ripening seems intuitively incongruous with experimental conditions that maintained high levels of supersaturation. Ostwald ripening has been presumed to occur at low levels of supersaturation, where the smallest crystals are unstable due to their high specific surface energy (e.g., Baronnet, 1982). However, the mechanism can be understood by considering data given by Morse and Mackenzie (1990) that show an inverse log relation between particle size and solubility for calcite. Alternatively, $K_{sp}$ and consequently $\Omega$ (Eqn. 3) as a function of size can be calculated from free

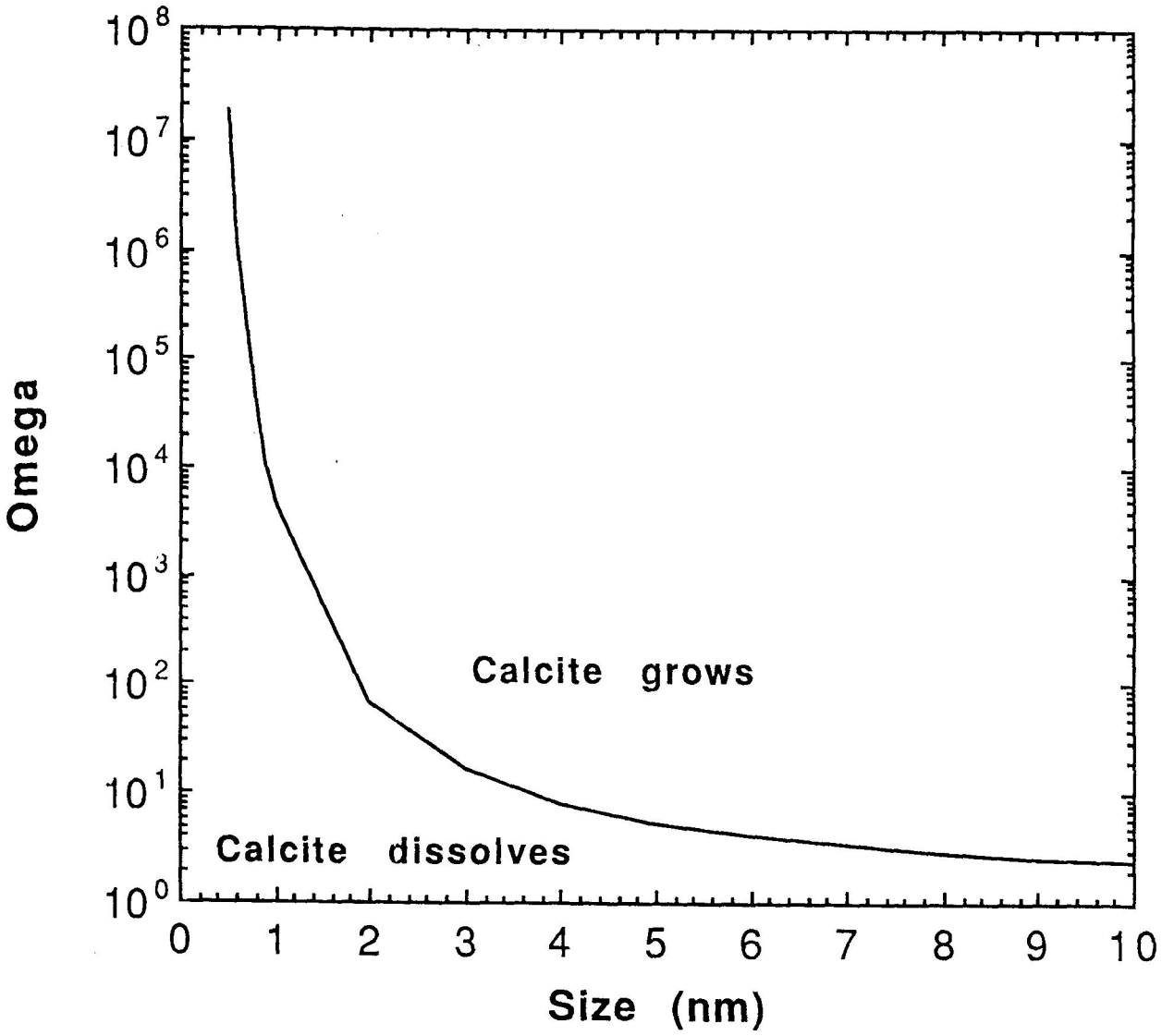


Fig. 10. Solubility of calcite vs. crystal size. The Ω axis is presented with respect to an infinitely large crystal, and the calculation for the curve includes the effects of surface-free energy on the calculation. The value for the surface-free energy for $CaCO_3$ used in the calculation is from Stumm (1992), and values for other free energies (see Eqn. 3) are from Garrels and Christ (1965).

energies for the species represented in Eqn. 4 (Garrels and Christ, 1965) and from the surface free energy for calcite of 94 $mJm^{-2}$ given by Stumm (1992). A plot of Ω (which is presented in Fig. 10 as the ratio of the size-dependent solubility product to the solubility product for an infinitely large crystal) as a function of crystal size indicates that very small crystals may dissolve even at high levels of supersaturation (with respect to an infinitely large crystal), and thereby contribute to the ripening process. For example, at a nominal Ω of approximately 3000 (see Table 1), crystals smaller than 1 nm may dissolve, whereas at an Ω of approximately 100 (the maximum attainable level of supersaturation according to Söhnel and Mullin, 1987), crystals smaller than 2 nm may dissolve. Consequently, Ostwald ripening may occur in systems having rapid nucleation kinetics because three factors ensure that numerous crystals occur simultaneously in this "sensitive" size range: (1) the smallest crystals are extremely small because the size of the critical nucleus formed during nucleation decreases with increasing levels of supersaturation (Walton, 1967; Stumm, 1992); (2) most of these small crystals have nucleated simultaneously because the nucleation rate increases with increasing supersaturation (Stumm, 1992); and (3) most of the smallest crystals have not grown beyond the sensitive size range because the rate of LPE growth decreases as crystal size decreases. Therefore, this type of Ostwald ripening must happen very early in the crystal growth process, at large initial values of Ω, in response to falling levels of supersaturation (caused by continued crystal growth), during which there were many crystals less than about 3 nm in size within the system to dissolve and thereby sustain the process.

Conversely, larger (and less soluble) nuclei which form at lower levels of supersaturation are less subject to ripening. For example, critical nuclei less than 3 nm are not expected to form in solutions having values of $\Omega < 20$ (Fig. 10 and Table 1). Moreover, a slower nucleation rate in such systems would lead to a predominance of LPE growth as the nucleation rate decays, thereby resulting in lognormal CSDs.

Earlier crystal growth theories (e.g., Dunning, 1961; Söhnel and Garside, 1992) postulated that the shape of the Ostwald curve (Fig. 4C), here attributed to Ostwald ripening, resulted from a single nucleation event that died out, and then was followed by a period where all crystals grew at the same rate. This explanation seems improbable, because by this mechanism systems having different rates of crystal growth and different crystal population densities would be expected to yield different CSD profiles. Five of our experimental systems, each having different experimental conditions (Table 1), yielded the same reduced CSD profile, a unique shape which fits that expected for Ostwald ripening.

The transitional plots shown in Figs. 5 and 6 further substantiate the hypothesis that it is initial solution saturation state (i.e., $\Omega$) that controls the degree of ripening. In contrast to the Ostwald CSDs in Figure 4 (in which the initial $\Omega$ values were in excess of about 100), these plots, with $\Omega$ ranging from approximately 28 to 69 (Table 1), show less of a shift from the lognormal toward the Ostwald curve, which indicates less ripening. The extent of the right shift of the curve maximum can be correlated approximately to the initial solution concentration. The shapes of the transitional CSDs were simulated using the Galoper program by assuming a decaying nucleation rate followed by Ostwald ripening (Fig. 5).

The presence of supply-controlled LPE growth, which does not have a specific CSD shape of its own, can be inferred from the previously described crystal growth experiments, because nucleation, surface-controlled LPE growth, and Ostwald ripening can occur in these systems only in the nanometer size range, whereas the experimentally measured mean sizes are three orders of magnitude larger. Supply-controlled growth, during which most of the mass of the crystals is added, mandates that the relative shapes and variances of the distributions, formed at small sizes, are maintained as all of the crystals grow at approximately the same proportional rate (Eberl et al., 1998). In other words, during supply-controlled growth, if the mean doubles in size, then all of the crystals in the system also double in size. It is because of this preservation of relative CSD shapes that conditions of early nucleation and crystallization can be inferred based on observed CSDs.

This point is illustrated in Table 2 and in Figure 7 for continuous-growth lognormal (CCNG 42 to 44) and Ostwald ripened (CCNG-19 and CCP-4) experiments, where $\beta^2$ remains relatively constant over as much as a 2.5-fold increase in crystal size for extended growth of the same sample. If sample CCNG-42, with a mean size of 8.5 $\mu$m and a $\beta^2$ of 0.30, had grown to the size of sample CCNG-44, with a mean size of 17.8 $\mu$m and approximately the same $\beta^2$ (0.36), by McCabe's law ($dX/dt = k$), Galoper calculations show that the CSD would have lost its lognormal shape and would have developed a $\beta^2$ of 0.07. Likewise, based on McCabe's law, CCP-4 crystals grown from seed crystals from the CCNG-19 experiment would have yielded a CSD which no longer fit the universal steady-state curve, and which had a $\beta^2$ of 0.03. Thus, it can be concluded that size-dependent growth ($dX/dt = kX$), rather than McCabe's law, prevailed in these experiments. However, under some experimental conditions, such as without stirring, non–size-dependent growth may predominate (e.g., McCabe and Stevens, 1951).

CSD shapes observed for synthetic calcite also may occur in nature. For example, the lognormal CSDs for calcite crystals from southeastern Colorado (Fig. 9) can be explained by a mechanism that is governed initially by surface-controlled (LPE) growth, followed by a longer period of supply-limited growth, during which the initially established lognormal shape is preserved during an increase in mean crystal size. The change from surface- to supply-controlled growth kinetics presumably resulted from an exponential increase in the demand for reactants (which is required to maintain LPE growth) that eventually exceeded the rate of nutrient supply provided by the system. The lognormal CSD is common in the geologic record (Eberl et al., 1998, and references therein; Kile and Eberl, 1999), and determination of the growth mechanism based on such CSDs may be used to infer geologic conditions early in the growth history of crystals.

## 6. CONCLUSIONS

Three basic shapes for calcite CSDs were realized in these experiments: asymptotic, lognormal, and Ostwald. Experimental conditions required to produce these three shapes are consistent with previously proposed mechanisms that can simulate these shapes: constant-rate nucleation and LPE growth (asymptotic CSD); decaying nucleation rate and LPE growth (lognormal CSD); and Ostwald ripening (Ostwald CSD, characterized by a unique negative skew). These CSD shapes were maintained during subsequent supply-controlled growth, when most of the mass of the crystals was added. Therefore, it may be possible to infer early environments of crystallization for natural calcite and other minerals from the shapes of their CSDs. This approach also could be used as a guide to control CSD shape during industrial crystallization.

*Acknowledgements*—Alex Blum (U.S. Geological Survey), Kathy Nagy (University of Colorado), John Neil (University of California, Davis), and Duncan Sibley (Michigan State University) provided manuscript reviews. The authors thank D. W. Rutherford for providing the calcite surface area determination by the BET method. The use of trade and product names in this paper is for identification purposes only, and does not constitute endorsement by the U.S. Geological Survey.

## REFERENCES

Arvidson R. S. and Mackenzie F. T. (1999) The dolomite problem: Control of precipitation kinetics by temperature and saturation state. *Am. J. Sci.* **299,** 257–288.

Ball J. W. and Nordstrom D. K. (1991) *User's Manual for WATEQ4F, with Revised Thermodynamic Data and Test Cases for Calculating Speciation of Major, Trace and Redox Elements in Natural Waters.* USGS Open-File Report, 91-183.

Baronnet A. (1982) Ostwald ripening: The case of calcite and mica. *Estudios Geologicos* **38,** 185–198.

Berglund K. A., Kaufman E. L., and Larson M. A. (1983) Growth of contact nuclei of potassium nitrate. *AIChE J.* **29,** 867–869.

Berner E. and Berner R. (1996) *Global Environment: Water, Air and Geochemical Cycles.* Prentice Hall.

Busenberg E. and Plummer L. N. (1986) A comparative study of the

dissolution and crystal growth kinetics of calcite and aragonite. In *Studies in Diagenesis* (ed. F. A. Mumpton), pp. 139–168. U.S. Geological Survey Bulletin 1578.

Canning T. F. and Randolph A. D. (1967) Some aspects of crystallization theory: Systems that violate McCabe's delta L law. *AIChE J.* **13,** 5–10.

Carrucio F. T. and Geidel G. (1978) Geochemical factors affecting coal mine drainage quality. *Reclamation of Drastically Disturbed Lands.* ASA-CSSA-SSSA.

Cashman K. V. and Marsh B. D. (1988) Crystal size distribution (CSD) in rocks and the kinetics and dynamics of crystallization: II. Makaopuhi lava lake. *Contrib. Mineral. Petrol.* **99,** 292–305.

Cashman K. V. and Ferry J. M. (1988) Crystal size distribution (CSD) in rocks and the kinetics and dynamics of crystallization: III. Metamorphic crystallization. *Contrib. Mineral. Petrol.* **99,** 401–415.

Davis R. V., Carter P. W., Kamrath M. A., Johnson D. A., and Reed P. E. (1995) The use of modern methods in the development of calcium carbonate inhibitors for cooling water systems. In *Mineral Scale Formation and Inhibition* (ed. Z. Amjad), Plenum Press.

Diehl H. (1964) *Calcein, Calmagite, and σ, σ'-Dihydroxyazobenzene Titrimetric, Colorimetric, and Fluorometric Reagents for Calcium and Magnesium.* G. Frederick Smith Chemical Co.

Drever J. I. (1997) *The Geochemistry of Natural Waters,* 3rd ed. Prentice Hall.

Dunning W. J. (1961) The physical and chemical production of powders by controlled precipitation. In *Powders in Industry,* pp. 29–40. Society of Chemical Industry Monograph 14.

Eberl D. D., Drits V. A., and Środoń J. (1998) Deducing growth mechanisms for minerals from the shapes of crystal size distributions. *Am. J. Sci.* **298,** 499–533.

Exner H. E. and Lukas H. L. (1971) The experimental verification of the stationary Wagner-Lifshitz distribution of coarse particles. *Metallography* **4,** 325–338.

Garrels R. M. and Christ C. L. (1965) *Solutions, Minerals and Equilibria.* Freeman, Cooper.

Garside J. and Jančić S. J. (1976). Growth and dissolution of potash alum crystals in the subsieve size range. *AIChE J.* **22,** 887–984.

Gibrat R. (1930) Une loi des répartitions économiques: L'effet proportionnel. *Bulletin Statist. Gén.* **19,** 469–513.

House W. A. (1981) Kinetics of crystallization of calcite from calcium bicarbonate solutions. *J. Chem. Soc. Faraday Trans. 1,* **77,** 341–359.

Isopescu R., Mocioi M., Zahanagiu F., and Filipescu L. (1996) Growth rate models and kinetics estimation for $CaCO_3$ precipitated in continuous crystallizers. *J. Crystal Growth* **167,** 260–264.

Kapteyn J. C. (1903) *Skew Frequency Curves in Biology and Statistics.* Noordhoff, Groningen, Astronomical Laboratory.

Kazmierczak T. F., Tomson M. B., and Nancollas G. H. (1982) Crystal growth of calcium carbonate: A controlled composition kinetic study. *J. Phys. Chem.* **86,** 103–107.

Kerrick D. M., Lasaga A. C., and Raeburn S. P. (1991) Kinetics of heterogeneous reactions. In *Contact Metamorphism* (ed. D. M. Kerrick), pp. 583–671. *Reviews in Mineralogy,* Vol. 26, Mineralogical Society of America.

Kile D. E. and Eberl D. D. (1999) Crystal growth in miarolitic cavities in the Lake George ring complex and vicinity, Colorado. *Am. Mineral.* **84,** 718–724.

Kitano Y. (1962) The behavior of various inorganic ions in the separation of calcium carbonate from a bicarbonate solution. *Bulletin Geochem. Soc. Japan* **35,** 1973–1980.

Kotaki Y. and Tsuge H. (1990) Reactive crystallization of calcium carbonate in a batch crystallizer. *J. Crystal Growth* **99,** 1092–1097.

Krumbein W. C. and Graybill F. A. (1965) *An Introduction to Statistical Models in Geology.* McGraw-Hill.

Larson M. A., White E. T., Ramanarayanan K. A., and Berglund K. A. (1985) Growth rate dispersion in MSMPR crystallizers. *Am. Inst. Chem. Engin. J.* **31,** 90–94.

Lifshitz I. M. and Slyozov V. V. (1961) The kinetics of precipitation from supersaturated solid solutions. *J. Phys. Chem.* **19,** 35–50.

Makowitz A. and Sibley D. F. (1999) Crystal growth mechanisms of quartz overgrowths in a Cambrian quartz arenite. In *Abstracts with Programs* **31,** Annual Geological Society of America Meeting, Oct. 1999, Denver, CO, p. A-282.

Marsh B. D. (1988) Crystal size distribution (CSD) in rocks and the kinetics and dynamics of crystallization: I. Theory. *Contrib. Mineral. Petrol.* **99,** 277–291.

Marsh B. D. (1998) On the interpretation of crystal size distributions in magmatic systems. *J. Petrol.* **39,** 553–599.

McCabe W. L. (1929) Crystal growth in aqueous solutions. *Ind. Engin. Chem.* **21,** 30–33.

McCabe W. L. and Stevens R. P. (1951) Rate of growth of crystals in aqueous solutions. *Chem. Engin. Prog.* **47,** 168–174.

Milliman J. D., Troy P. J., Balch W. M., Adams A. K., Li Y.-H., and Mackenzie F. T. (1999) Biologically mediated dissolution of calcium carbonate above the chemical lysocline? *Deep-Sea Research I* **46,** 1653–1669.

Morse J. W. and Mackenzie F. T. (1990) *Geochemistry of Sedimentary Carbonates.* Developments in Sedimentology No. 48, Elsevier Publ.

Nielsen A. E. (1964) *Kinetics of Precipitation.* Pergamon Press.

Nordeng S. H. and Sibley D. F. (1996) A crystal growth rate equation for ancient dolomites: Evidence for millimeter-scale flux-limited growth. *J. Sediment. Res.* **66,** 477–481.

Parkhurst D. L. (1995) *User's Guide to PHREEQC: A Computer Program for Speciation, Reaction-Path, Advective-Transport, and Inverse Geochemical Calculations.* Water Resources Investigations Report 95-4227.

Randolph A. D. and Larson M. A. (1988) *Theory of Particulate Processes,* 2nd ed. Academic Press.

Reddy M. M. (1986) Effect of magnesium ions on calcium carbonate nucleation and crystal growth in dilute aqueous solutions at 25°C. In *Studies in Diagenesis* (ed. F. A. Mumpton), pp.169–182. U.S. Geological Survey Bulletin 1578.

Reddy M. M. and Nancollas G. H. (1976) The crystallization of calcium carbonate. *J. Crystal Growth* **35,** 33–38.

Ridgley J. L. (1986) Diagenesis of the Todilto Limestone member of the Wanakah Formation, Chama Basin, New Mexico. In *Studies in Diagenesis* (ed. F. A. Mumpton), pp. 197–206. U.S. Geological Survey Bulletin 1578.

Söhnel O. and Garside J. (1992) *Precipitation, Basic Principles and Industrial Applications.* Butterworth-Heinemann Ltd.

Söhnel O. and Mullin J. W. (1987) Interpretation of crystallization induction periods. *J. Colloid Interface Sci.* **123,** 43–50.

Spanos N. and Koutsoukos P. G. (1998) Kinetics of precipitation of calcium carbonate in alkaline pH at constant supersaturation. Spontaneous and seeded growth. *J. Phys. Chem. B,* **102,** 6679–6684.

Stumm W. (1992) *Chemistry of the Solid Water Interface.* Wiley, New York.

Tai C. Y., Chen P-C., and Shih S-M. (1993) Size-dependent growth and contact nucleation of calcite crystals. *AIChE J.* **39,** 1472–1482.

Tai C. Y. and Yu K. H. (1989) Growth kinetics of potassium alum crystal in a well- agitated vessel. *J. Crystal Growth* **96,** 849–855.

Tomson M. B. and Nancollas G. H. (1978) Mineralization kinetics: A constant composition approach. *Science* **200,** 1059–1060.

Wagner C. (1961) Theorie der Alterung von Neiderschlägen durch Umlösen (Ostwald Reifung). *Zeitschrift fuer Elektrochemie,* **65,** 581–591.

Walton A. G. (1967) *The Formation and Properties of Precipitates.* Interscience Publ.

White E. T. and Wright P. G. (1971) Magnitude of size dispersion effects in crystallization. In *Crystallization from solution: Factors influencing size distribution* (ed., M. A. Larson), pp. 81–87. American Institute of Chemical Engineers, Vol. 67.

Winter B. L., Valley J. W., Simo J. A., Nadon G. C., and Johnson C. M. (1995) Hydraulic seals and their origin: Evidence from the stable isotope geochemistry of dolomites in the middle Ordovician St. Peter Sandstone, Michigan Basin. A.A.P.G. Bulletin 79.